Heliyon 5 (2019) e01984

Contents lists available at ScienceDirect

Heliyon

journal homepage: www.heliyon.com

Screen printed carbon electrode sensor with thiol graphene quantum dots and gold nanoparticles for voltammetric determination of solatol

Mahmoud Roushani [a,*], Zeynab Jalilian [b], Azizollah Nezhadali [b]

[a] Department of Chemistry, Ilam University, Ilam, Iran
[b] Department of Chemistry, Payame Noor University, PO.Box19395-4697, Tehran, Iran

ARTICLE INFO

Keywords:
Analytical chemistry
Electrochemistry
Thiol graphene quantum dots
Modified electrode
Molecularly imprinted polymer
Sotalol

ABSTRACT

This work, a highly selective and sensitive sensor is described for voltammetric determination of the sotalol (SOT). The dual actions of sotalol lead to reductions in the automaticity of myocardial cells and in conduction through the atrioventricular node. Drug analysis has an extensive impact on public health. The molecularly imprinted sensor was constructed by modifying a screen printed carbon electrode (SPCE) with thiol graphene quantum dots (GQD-SH) and gold nanoparticles (AuNPs). Under optimal conditions the nanotools has a dynamic range that covers the 0.1–250 μM SOT concentration range, and the detection limit is 0.035 μM. This is lower than any of the previously reported methods. The MIP-sensor also exhibited excellent selectivity, good stability and adequate reproducibility for the detection of the SOT over its structural analogs. The prepared sensor was successfully applied to the measurement of SOT in various real samples including tablet and human blood serum.

1. Introduction

Sotalol (SOT), N-{4-[1-hydroxy-2-(propan-2-ylamino) ethyl] phenyl} methane sulfonamide (see Scheme 1), is a new category of antiarrhythmic drugs with ß-adrenergic receptor blocking properties. It is a quick non-selective receptor antagonist for all sorts of life-threatening ventricular arrhythmia [1,2]. It is used for cure of hypertension, ischemic heart disease, congestive heart failure, and certain arrhythmias. For pharmacokinetic studies of this drug and more routinely for establishing a relationship between blood concentration and therapeutic effect [3] or toxic influence [4], the measurement of plasma or serum is necessary. For analysis of SOT in biological matrices, some analytical methods have been reported including voltammetry and other methods [2,3,5,6,7,8,9].

Molecularly imprinted polymer (MIP) is a form of synthesized material, which is usually prepared by the copolymerization of a function monomer and cross-linker when the template is present. In the following, the analyte molecules are removed from the final polymer matrixes and providing binding sites preferably matching in size, shape, and functionality to the template [10]. Binding sites can specifically distinguish the template. In last years, electrochemical methods, especially electrochemical MIP based sensors, have caught more attention because of their recognition properties, good selectivity, excellent sensitivity, simplicity, high stability, fast response, low cost, and real time detection [11,12,13,14,15].

Currently, screen printed electrodes (SPEs), with low cost, simple, inexpensive and speed of mass production using thick film technology have been extensively used for developing novel (electrochemical) sensing platforms and improving their performances [16]. Generally, SPEs are fabricated by printing diverse electroconductive and insulative inks on a plastic or ceramic substrate and the printed inks can be synthesized with different compositions and conditions, thereby causing wide flexibility and versatility of the SPCEs for pragmatic use [17,18]. Many kinds of metal nanoparticles organic compounds, and nano composites have been applying to modify the SPC electrode surface [17,19,20].

In recent years, special notice has been taken to nanoparticles particularly regarding metallic nanoparticles (NPs) such as AuNPs, with heightened behavior in electrochemical analysis due to their large effective surface area, excellent conducting capability, fast mass transport and effective catalysis [20,21]. In this survey, the AuNPs were located onto the surface of modified SPCE to extend the electrochemically active sites and make easy the electron transfer from the reaction center to the electrode surface [17,19,21].

GQDs are one or few-layered grapheme sheets with lateral size smaller than 100 nm in single double and multiple layers [22,23]. The GQDs are anticipated to have the important properties due to quantum detention and edge effects, making it an excellent candidate for

* Corresponding author.
E-mail address: m.roushani@ilam.ac.ir (M. Roushani).

https://doi.org/10.1016/j.heliyon.2019.e01984
Received 30 March 2019; Received in revised form 23 May 2019; Accepted 18 June 2019

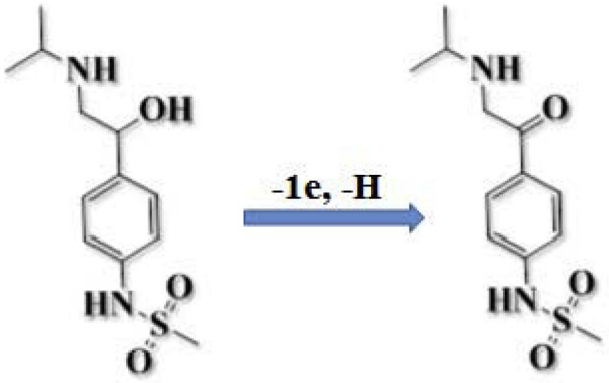

Scheme 1. The mechanism of electrooxidation of SOT.

construction nanoscaled optical, magnetic and electronic tools [24,25, 26]. This is recently reported that the GQDs are applicable in various branches such as immunoassays, enzyme based bioanalysis, drug carrier, photoluminescence and also electrochemical methods [27,28,29]. Some GQDs, such as thio-GQDs (SH-GQD) are a category of quantum dots. They were discovered to form firm colloidal suspensions in different solvents. However, the water solubility of the SH-GQD is less than the water solubility of the ox-GQD [30]. Herein, for the first time we established a facile green method to use the AuNPs, the GQD-SH and the MIP as the nanomaterial to the surface of SPCE for selective and ultrasensitive determine of the SOT.

2. Experimental

2.1. Material and reagents

Analytical reagent grade such as azobisisobutyronitrile (AIBN), Methacrylic acid (MAA), Tetrachloroauric acid ($HAuCl_4$) and sodium citrate ($Na_3C_6H_5O_7.2H_2O$), ethylene glycol dimethacrylate (EGDMA) and all other reagents were bought from KimiaExir chemical companies (Tehran, Iran). Sotalol hydrochloride was contributed by farabi Darou (Isfahan, Iran). The 0.04 M Britton-Robinson (BR) buffer solution pH 7 was practical as a supporting electrolyte.

2.2. Apparatus

The whole of electrochemical experimental accomplish with a μ-AUTOLAB electrochemical system driven with NOVA software. The pH was measured by a Metrohm model, 780 pH/mV meters. A screen-printed carbon electrode (SPCE) (3 mm in diameter) bought from Dropsens (Spain) was used as a planar three electrode based on a graphite working electrode, a silver pseudo-reference electrode and a carbon counter electrode. DPV and CVs measurements were performed in 0.04 mol L^{-1} Britton-Robinson (BR) solution. Moreover, electrochemical impedance spectroscopy (EIS) was recorded in 0.5 mol L^{-1} KCl solution containing 5 mM $Fe(CN)_6^{4-/3}$. Surface morphology of the imprinted polymer particles were considered by using FESEM (Model: Hitachi S4160).

2.3. Synthesis of MIP-polymer

2.3.1. Synthesis of polymer

For synthesize SOT-MIP-polymer, we used the reported method in ref [13] and for this synthesis, the following steps are followed; at first the template molecule (SOT, 1 mmol) and functional monomers MAA (4 mmol) were dissolved in 40 mL acetonitrile as solvent and then sonicated for 10 min. Subsequently, 2,2-azobisisobutyronitrile (AIBN, 1.0 mmol) and 25.0 mmol of EGDMA as a cross-linker agent were added and the mixture was purged with nitrogen for 10 min and then the reaction mixture was refluxed in an oil bath (stirring speed of 400 rpm and 60 °C) for 24 h in the following, the nanoparticles were collected and washed with ethanol, respectively to remove additional reagents and solvent. The SOT and unreacted monomers were removed through washing of the polymer with methanol–acetic acid (9:1, v/v) solution for several times. At the last, particles were collected and then were washed by double distilled water until neutral pH is reached and dried at 60 °C and stored for more use. Non imprinted polymers (NIPs) were ready similar to over suggestion conditions but without of SOT.

2.4. Synthesis of gold nanoparticles (AuNPs)

Gold nanoparticles were provided based on an already report as described in ref [17] and details of this synthesis completely explained in the following. Gold nanoparticles were synthesized in four stages: i) First, 500 mL tetrachloroauric acid (0.01% (w/v), HAuCl4) was heated with stirring to reach boiling point. ii) During stirring, quickly 7.5 mL of a 1% solution of trisodium citrate dehydrate aqueous (Na3C6H5O7–2H2O) was added to this solution. iii). After 25 s, the color of the solution was turned into blue and, finally, after 70 s the color was turned into red-violet. iv) boiling went on for an additional 10 min v) the heating was stopped and the colloid was stirred for another 15 min. The obtained solution was transparent red and AuNPs had no precipitate and the particles were about 12 nm. After cooling, the solution was kept in refrigerator at 4 °C until it was ready to be used.

2.5. Synthesized of SH-GQD

Thio-GQDs were synthesized based on an already report as described in ref [30] and details of this synthesis completely explained in the following. For this synthesis of GQD-SH, Briefly, 0.1 g MWCNTs powder was added to 10 mL of HNO3/H2SO4 mixture at a ratio of 1:3 and was sonicated for 6 h at 40 °C to yield oxidized MWCNTs (ox-MWCNTs). The obtained black suspension containing ox-MWCNTs was diluted with distillated water and allowed to stand overnight for precipitation. Then the supernatant was removed and the suspension of ox-CNT was diluted with deionized water and filtered with a 0.05 mm filter membrane under vacuum. In order to form a stable colloidal suspensions the ox-CNT were dissolved in a plenty of solvents including water, ethanol and dimethylformamide. 1 mL of 1 mmol L-1 cysteamine solution in ethanol was added to the resulted suspension, mixed (24 h) and then decanted overnight. Cysteamine leads to isolating of NPs which is named as oxidized GQD (ox-GQD) on the CNTs suspension. 10 mmol L-1 of DCC solution in DMF was added to the collected ox-GQD to start the coupling reaction and it was mixed for 24. Finally, the GQD were purified by repeated filtration through a cut-off membrane (MW 1500) and rinsed with fresh DMF. In this way GQD-SH was achieved.

2.6. Fabrication of MIP sensor

In this study beforehand use the SPCE, the electrode were ready by employment a potential of −0.4 to +1.5 V in HCl 0.10 M for 20 cycles by scan rate of 50 mv s^{-1} [17]. Then it could be cleaned with deionized water and dried before use. The electrode was modified by 5.0 μL of synthesized SH-GQD and dried for 60 min at room temperature under the lid. Afterwards, the modified SPC electrode surface covered by 5.0 μL of AuNPs solution for 30 min at room temperature under the lid until interaction between AuNPs and SH-GQD established. Subsequently, 5.0 μL of MIP was placed onto the surface of AuNPs/GQD-SH/SPCE and allowed to dry.

2.7. Preparation of the real samples

Survey the practicability of the sensor in practical analysis, the drug-free human serum was custom-made from a local clinical laboratory and centrifuged for 30 min by 5000 rpm. Subsequently, the serum samples

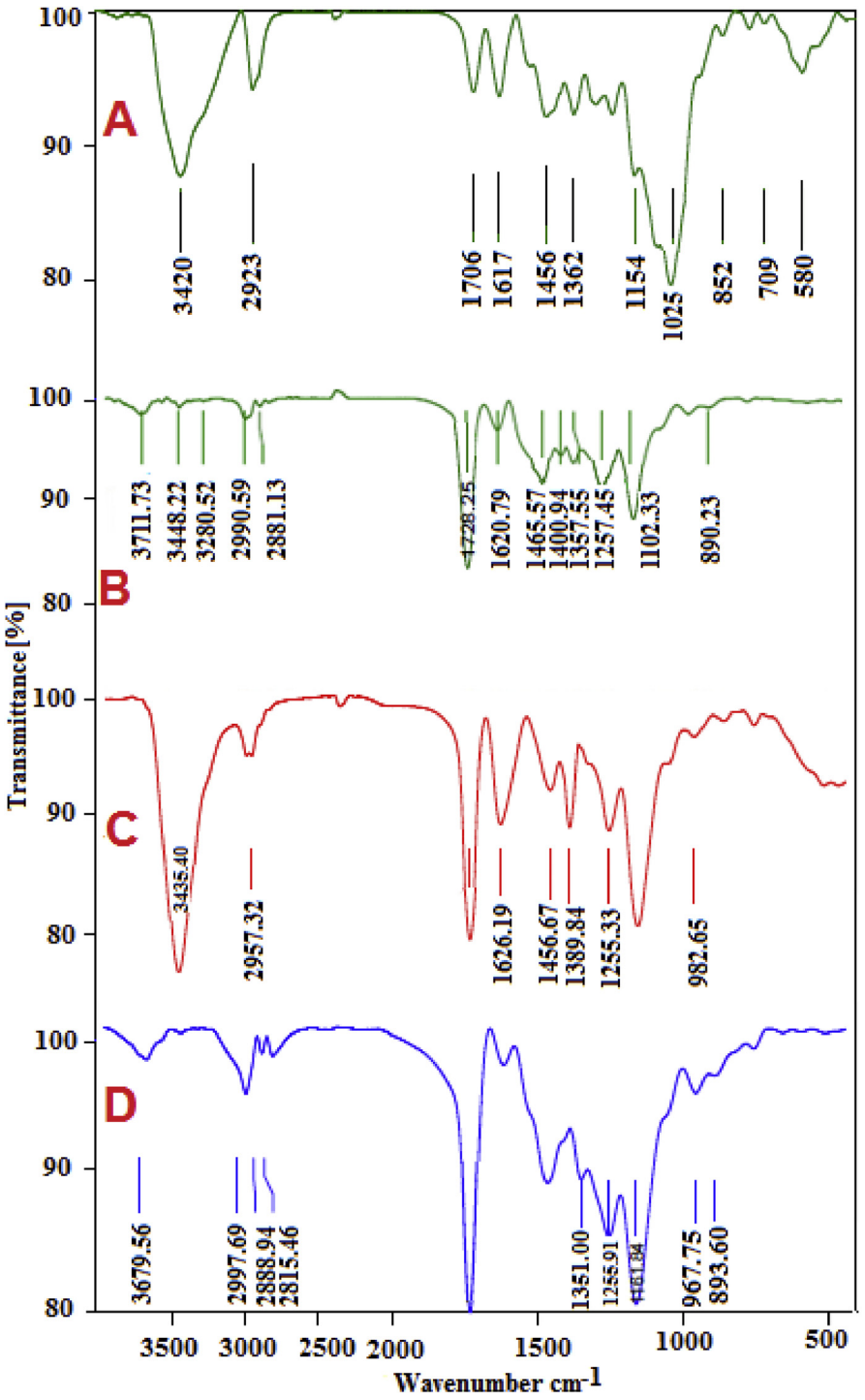

Fig. 1. The IR spectra of SOT (A) NIP (B) un-leached (C) and leached (D) SOT imprinted polymers.

were diluted 5 times with phosphate buffer solutions (0. 1M) and various concentrations of SOT were added to these samples.

In order to pharmaceutical analyses five tablets of SOT, labeled 80 mg per tablet (Hakim Darou Company, Iran), were weighed and crushed in a mortar to a fine powder. Amount of powder equivalent to the average mass of one tablet was dissolved in 25 ml of B-R (0.04 M, pH 10.0). Subsequently it was introduced to an ultrasonic bath for 15 min, filtered and diluted with the same buffer in a calibrated volumetric flask (100 ml). Finally, the prepared solution was transferred into the electrochemical cell and standard addition method was applied for the determination of SOT in tablet.

3. Results and discussion

3.1. Characterization of the NIP and MIP

To confirm the synthesized SOT-MIP the FT-IR spectra of SOT, NIP and also MIPs before and after the removal of SOT were recorded (Fig. 1).

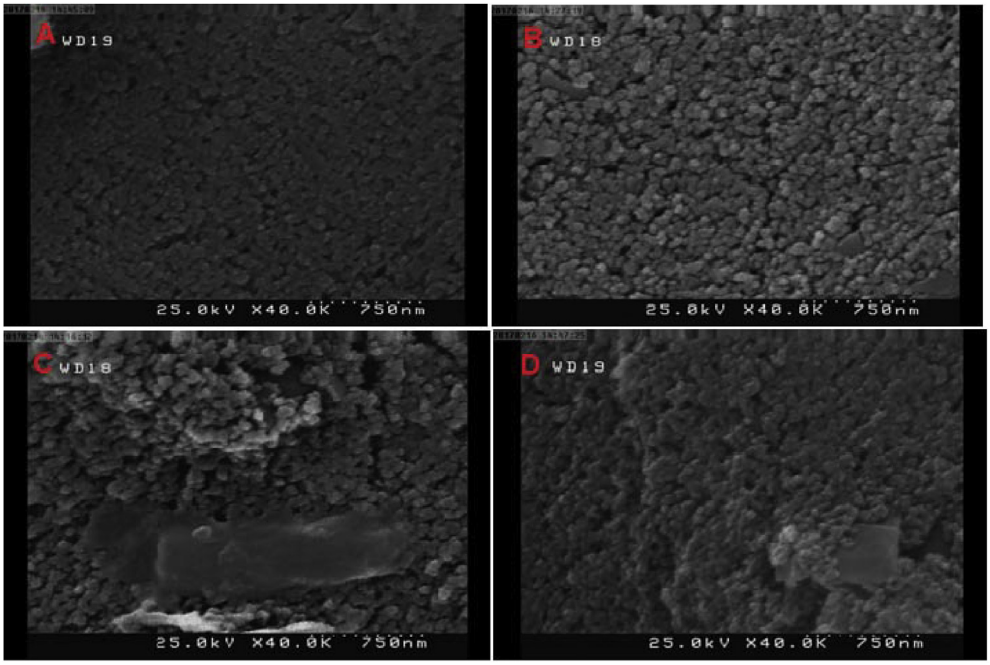

Fig. 2. SEM images of (A) bear SPCE, (B) MIP/GQD-SH/SPCE, (C) MIP/AuNPs/SPCE, and (D) MIP/AuNPs/GQD-SH/SPCE.

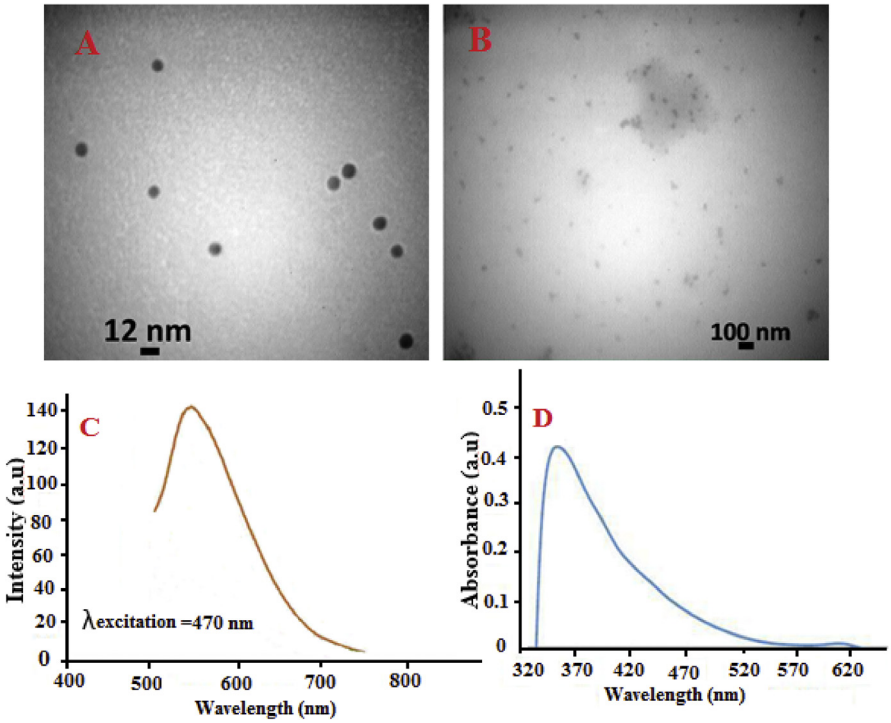

Fig. 3. (A) TEM image of the synthesized AuNPs and (B) TEM image of the synthesized thiol-GQD, (C) Florescence spectra and (D) UV-vis spectra of the synthesized thiol-GQD.

The IR spectrum of SOT indicated the stretching vibrations at 1154 cm^{-1} and 1362 cm^{-1} which corresponded to S=O symmetric and asymmetric stretching, respectively.

The presence of absorbance bands at 3420 and 3435 cm^{-1} were observe as double that maybe is impute to the N–H stretching vibration of $–NH_2$ group. In curve C the peak at 1732 cm^{-1} was attributed to C=O absorbance. The weak absorbance peak at 1628 cm^{-1} is corresponded to C=C and simultaneously indicated that most MAAs were cross-linked and alone a few ones remained. On the other hand, The –COOH group of MAA and the O–H stretching were discern based on their bending vibrations at 3435 cm^{-1} and 1389 cm^{-1}. Also, the features of the O–H banding were in 3435 cm^{-1} and it can be seen which at the MIP leached that the intensity of the peak was weaker and reached 3679 cm^{-1} shifts. Also, according to Fig. 1, we can say that the main band spectra of MIP unbleached and leached had the same position and form which could demonstrate that the analyte had been removed thoroughly from the MIP after washing.

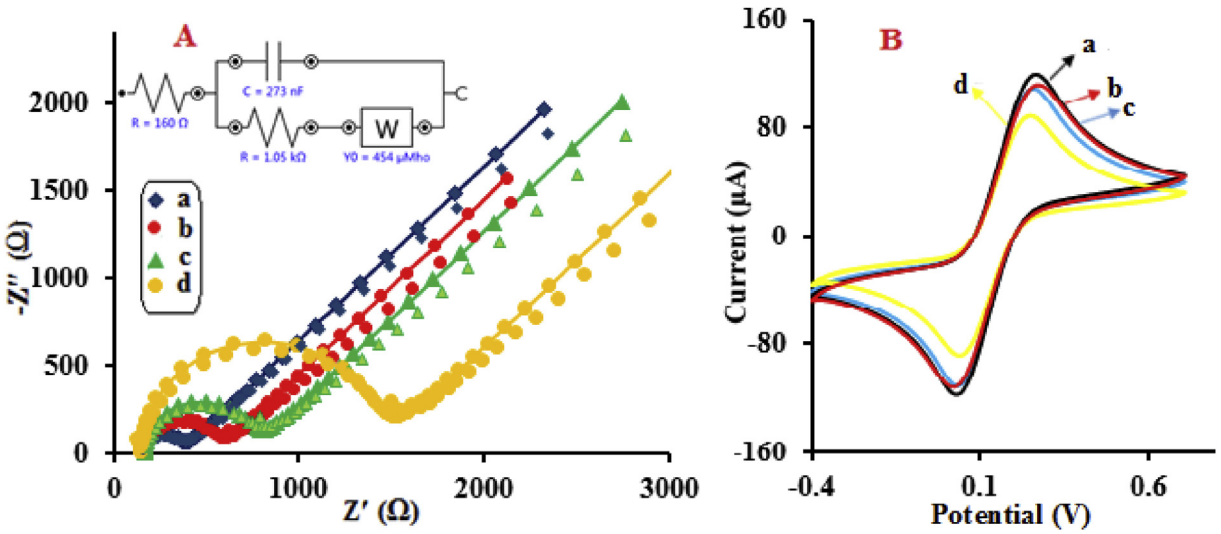

Fig. 4. Nyquist diagrams (A) and cyclic voltammograms (B) of the modified electrode after each immobilization (a) bear SPCE, (b) GQD-SH/SPCE, (c) AuNPs/GQD-SH/SPCE, (d) MIP/AuNPs/GQD-SH/SPCE, in $[Fe(CN)_6]^{-3/-4}$ as electrolyte solution.

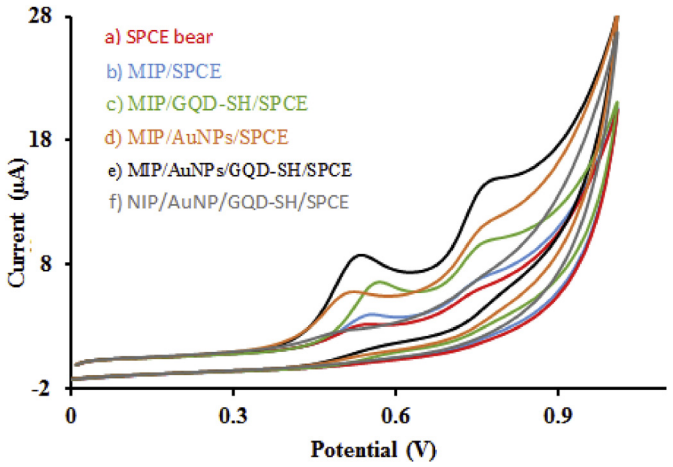

Fig. 5. Cyclic voltammograms of (a) bear SPCE, (b) MIP/SPCE, (c) MIP/GQD-SH/SPCE, (d) MIP/AuNPs/SPCE, (e) MIP/AuNPs/GQD-SH/SPCE, (f) NIP/AuNPs/GQD-SH/SPCE; after elution, in B-R buffer solution (pH 10) containing 100 μM SOT at the scan rate of 100 mV s^{-1}.

3.2. Scanning the electron microscopy (SEM) MIP/AuNPs/GQD-SH/SPCE

For assess the morphology and structure of prepared products we used SEM images (Fig. 2(A-D)). Fig. 2A showed SEM image of the bare electrode, which showed a smooth and uniform surface. As it was obvious in Fig. 2B that after dropped GQD-SH on the surface bear SPCE, scattered uniformly on the working electrode and had large surface area for the electron transfer. When the AuNPs dropped on the surface of electrode, the SEM images showed a uniform coverage of the AuNPs with small particles size on the surface of the GQD-SH/SPCE, which it possessed more sites for binding with the SH-GQD and this caused the increase interaction area and electron transfer rate on the surface of the electrode (Fig. 2C). It can be found rough and multi-hole structure in Fig. 2D, which ready a large recognition sites in removing the MIP/AuNPs/GQD-SH/SPCE.

3.3. Characterization of the synthesized thiol-GQD and AuNPs

For assess the structure of prepared products AuNPs and the SH-GQD we used TEM images. The TEM images in Figs. 3A and 3B confirm the formation nanomaterials, which promoted the charge transfer and could function as a desired modifier for enhancing the electrode surface area.

Also, the fluorescence spectra of the synthesized SH-GQDs was investigated (Fig. 3C). It can be observed that a maximum intensity in 470 nm. That in agreement with other some recent studies of the fluorescent of SH-GQDs [29].

Furthermore, UV-vis spectra of the synthesized SH-GQD were studied. As shown in Fig. 3D, the SH-GQDs had an absorbance intensity of 0.423.as likewise previous reports [29].

3.4. Characterization of the modified electrodes

The electrochemical behavior of different modified electrodes in each step was examined by recording of related CV and EIS in ferro/ferricyanide solution.

EIS as an efficient technique was used for monitoring the interface properties of modified electrodes during stepwise modifications. The Nyquist plots at unmodified SPCE, GOD-SH/SPCE, and AuNPs/GOD-SH/SPCE in 5 mM ferro/ferricyanide solution were shown in Fig. 4(A). As obvious in Fig. 4(A) (curve a) the spectrum represented an electrochemical impedance of the unmodified SPC electrode (R_{ct} = 400 Ω). Afterwards, with placed 5 μL of SH-GQD on the surface of bear SPCE (curve b), R_{ct} was increased to 622 Ω, via the thiol and hydroxyl groups in the compound of the SH-GQD. This was because of the negatively charged SH-GQD which was produced an electrostatic repulsion force to ferro/ferricyanide. In the next step, when 5 μL of the AuNPs placed onto the surface GQD-SH/SPCE the resistance for the redox probe clearly enhanced (R_{ct} = 831 Ω) (curve c) because, the AuNPs presence with negative charge on the electrode surface repelled the negatively charged ferro/ferricyanide to the extent that the response of probe was reduced and thus causes increased R_{ct}. Subsequently, when MIP was dropped on the surface of the AuNPs/GOD-SH/SPCE, Rct clearly increased (R_{ct} = 1537 Ω). This may be attributed by the non-conductive membrane formed by the monomers and SOT, which inhibited the transfer of electrons (curve d). Also, the sensor manufacture process was examined by recording cyclic voltammograms of the modified electrode during preparation steps in 5.0 mM ferro/ferricyanide solution (Fig. 4(B)). These results were accordant with CV diagrams as described in details above, corroborate that the proposed sensor worked indeed was achieved successfully.

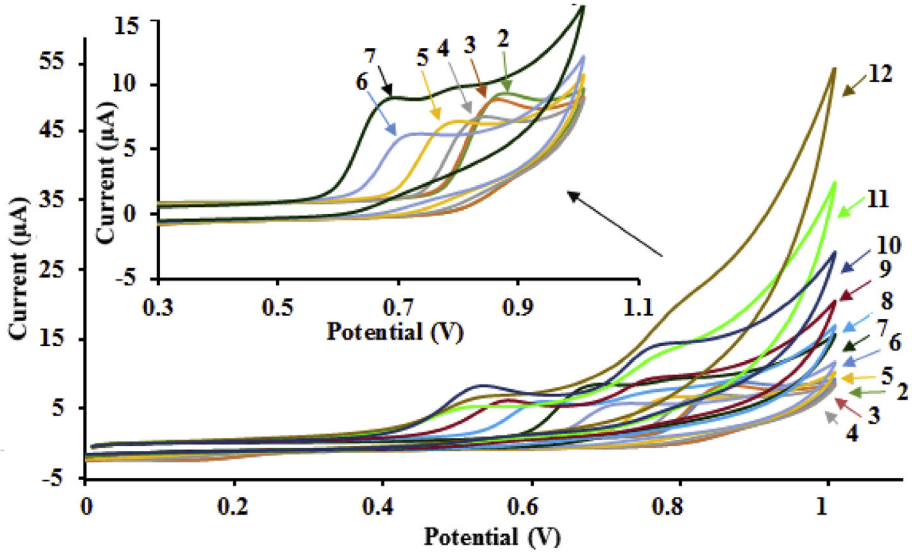

Fig. 6. Cyclic voltammetric response of the MIP/AuNPs/GQD-SH/SPCE electrode for 100 μM SOT at different pH values (a = 2 to j = 12) of B-R buffer solution at the scan rate of 50 mV s^{-1}. The inset shows plot of values (a = 2 to j = 7).

3.5. Electrocatalytic oxidation of SOT

To elucidate the direct electrochemistry behavior of SOT, cyclic voltammetric technique was used. Fig. 5 showed a typical cyclic voltammograms of diverse electrodes in B-R buffer solution (0.04 M, pH 10.0) in the attendance of 100.0 μM SOT with scan rate 50 mV s^{-1}. The outcomes confirmed that the bare SPCE in buffer solution in the attendance of 100.0 μM SOT displayed an irreversible redox peak for SOT, and the oxidation peaks of SOT was found at p1 = 0.540 and p2 = 0.750 V. The same irreversible behavior and shown two peaks had been reported in the previous reports [10]. As it was seen from (Fig. 5, curve b), after modification surface SPCE by 5 μL of MIP, small changes in the peak current obviously were seen for the MIP/SPCE. It can be seen that the peak current of SOT at the surface of the MIP/GQD-SH/SPCE (Fig. 5, curve c) was better than that for the MIP/SPCE and for the bare SPCE. In opposite, when the electrode SPCE was modified by the AuNPs and the MIP, the peak potentials of SOT shifted towards negatively potential values than that for the MIP/GQD-SH/SPCE (Fig. 5 curve d). This indicated a role of the AuNPs with an incremental surface area and conductivity of the resulted electrode (MIP/AuNPs/SPCE). Furthermore after placing the AuNPs on the surface GQD-SH/SPCE which it had more sites for binding with the SH-GQD, and subsequently the MIP as appropriate recognition element, developed the interaction area and increased the electron transfer rate on the surface of the electrode. The comparison of the peak intensity currents in all the tested electrodes showed that the higher peak current of SOT appeared on the MIP/AuNPs/GQD-SH/SPCE (curve e). In the other hand, in Fig. 5 (curve f) almost no electrochemistry response could be beheld with the NIP/AuNPs/GQD-SH/SPCE, eventuating from the blocking of electron transfer by the polymeric matrix covering the entire surface of the electrode.

3.6. Effect of pH

To achieve the best condition for the electrochemical oxidation, we studied the influence of pH on the electrochemical responses of SOT in the surface of proposed sensore in buffer solution with varying pH from 2.0 to 12.0 (Fig. 6). Whereas SOT at the surface of the MIP/AuNPs/GQD-SH/SPCE showed two peaks, several factors affected the peak currents and peak potentials. The results showed that, both the peak potentials of SOT shifted to negatively potential values as the solution pH increased (Fig. 6). Which it was an incontestable reality that protons represented a momentous participator in the oxidation procedure of SOT at the MIP/AuNPs/GQD-SH/SPCE. Additionally, according to equation Epa(V) = -0.0575 pH + 1.0706, which was the relationship between the potential and pH value and with respect to the slope of 57.5 mV/pH, it could be seen that the number of protons and electrons exchanged in the oxidation mechanism was equal. Nonetheless, at higher pH of 10.0, the electrical conductivity of the sensore reduced and it likewise could result in the decreases of the electrochemical responses of SOT at the MIP/AuNPs/GQD-SH/SPCE. In addition, as it is seen from Fig. 6 the best I_p was appeared, at pH 10.0. Hence, pH 10.0 was chosen for all the testing.

3.7. Effect of scan rate

The influence of scan rate (υ) on the electro-oxidation of SOT was likewise examined by varying the scan rate 5 to 100 (Fig. 7(A)). The signal achieved revealed that the both peak currents increased linearly with increasing the scan rate (υ) ($R^2_{(p1)} = 0.9944$, $R^2_{(p2)} = 0.9923$), that this consequence obviously indicated an adsorption-controlled electro-oxidative process. In addition, to obtain information about the rate-determining step, Tafel plot was depicted (Fig. 7(B)). Therefore, the value electron transfer coefficient (α) was almost $P_1 = 0.86$ and $P_2 = 0.9$ for the irreversible electrode process.

3.8. Effect of accumulation potential and accumulation time

Accumulation time and potential is an important parameters for enhancing the sensitivity of the imprinted sensor [22]. Hence, Influences of the accumulation time and the accumulation potential were investigated in buffer solution containing 100 μM SOT by the CV method. The accumulation time was changed from 10 s to 100 s. The results showed peak current enhanced meaningfully by the increase of the accumulation time to 100 s, and after the 70 s peak current reduced so, 70 s was used in the subsequent experiments (Fig. 8). Similarly, the dependence of the accumulation potential on the peak current of 50 μM SOT from −0.8 to 0.5 V was examined. The cyclic voltammograms in Fig. 9 corroborated that the extreme peak current took place at -0.6 V. Hence, for further study the accumulation potential of -0.6 V was chosen.

3.9. Analytical application

The equipped MIP/AuNPs/GQD-SH/SPCE as the proposed sensor based on the primary experimental results defined described in the preceding sections was fabricated. The typical DPV of sensor using 12

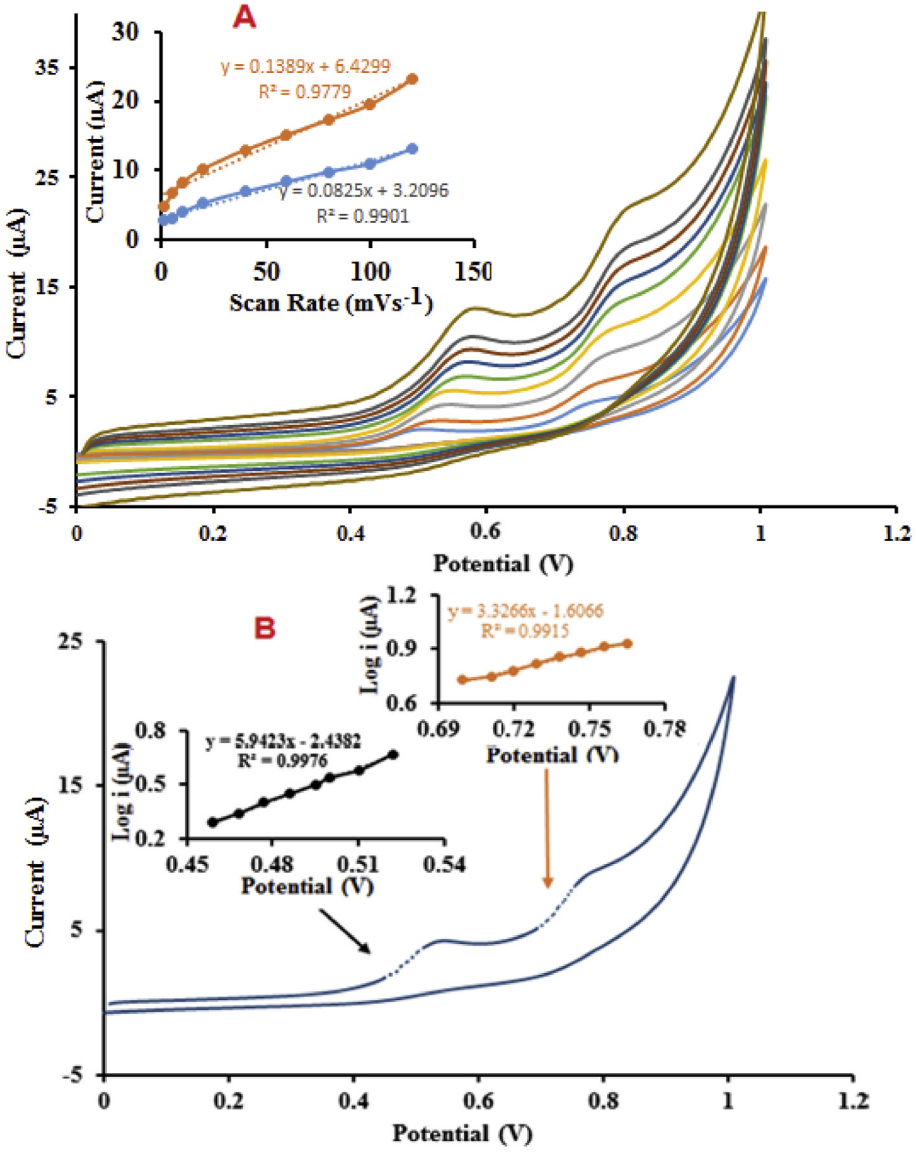

Fig. 7. A) Cyclic voltammograms of MIP/AuNPs/GQD-SH/SPCE in B-R buffer solution (pH 10) containing 100 µM SOT at various scan rates (5–100 mV s^{-1}). The inset shows plot of peak current *vs* scan rate. B) Tafel plot derived from the rising part of voltammogram recorded at the scan rate 20 mV s^{-1}.

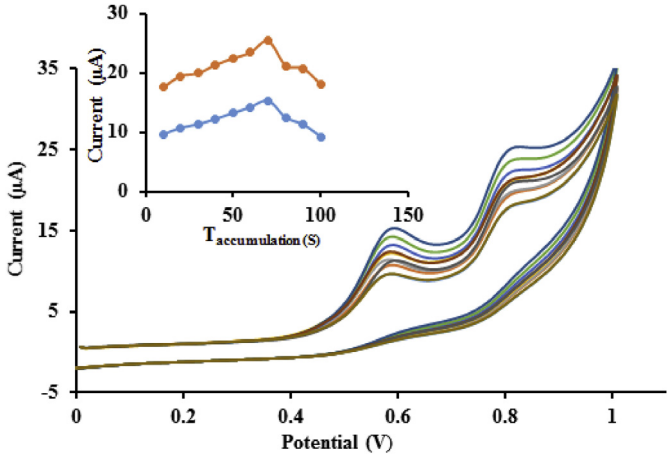

Fig. 8. Cyclic voltammograms of MIP/AuNPs/GQD-SH/SPCE in B-R buffer solution (pH 10) containing 100 µM SOT at various accumulation times of 10–100 s (at a scan rate of 50 mV s^{-1}). The inset shows plot of current *vs.* accumulation time.

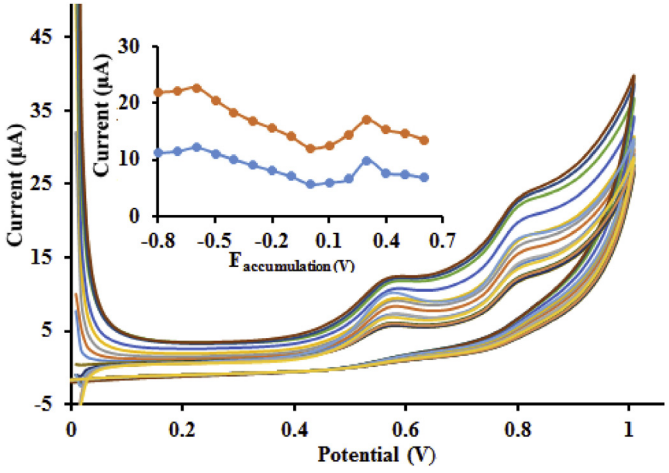

Fig. 9. Cyclic voltammograms of MIP/AuNPs/GQD-SH/SPCE in B-R buffer solution (pH 10) containing 100 µM SOT at various accumulation potential of -0.8 to 0.6 V (at the scan rate of 50 mV s^{-1}). The inset shows plot of current vs accumulation potential.

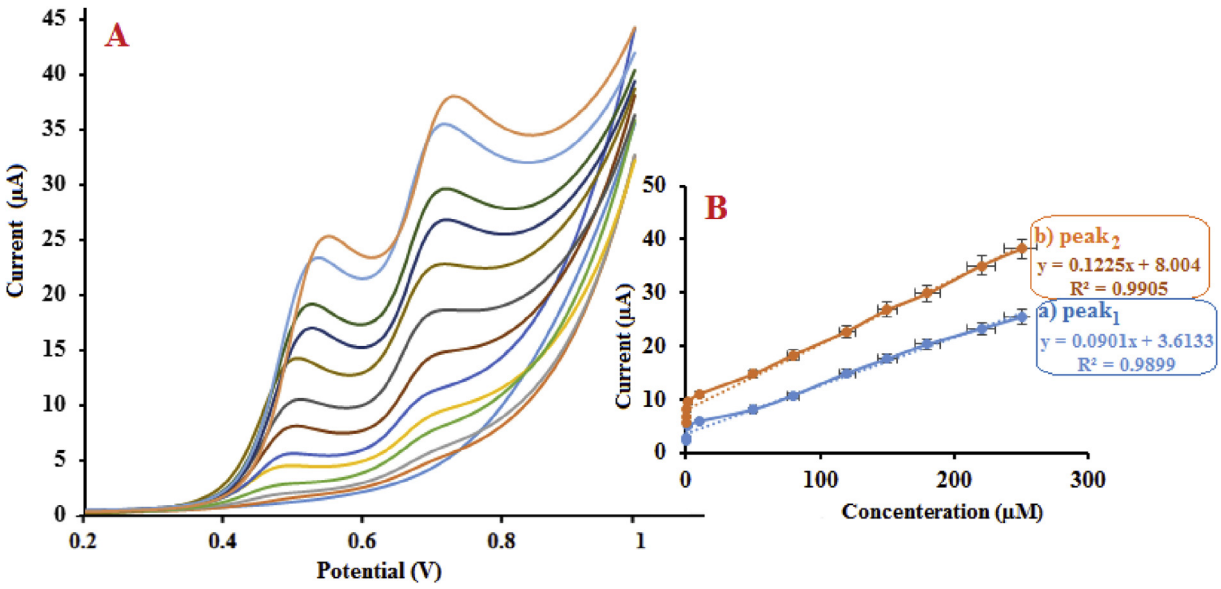

Fig. 10. A) DPV voltammograms of different concentrations of SOT at the MIP/AuNPs/GQD-SH/SPCE at optimized condition (t_{ac} = 70 s, E_{ac} = -0.6 V). B) The inset shows the corresponding calibration plot for the MIP/AuNPs/GQD-SH/SPCE.

Table 1
Comparison of proposed sensor with previously reported methods for detection of SOT.

Method	Modified Electrode	Limit of detection	Linear dynamic range	Ref.
CV	$NiFe_2O_4$/MWCNT/GCE	0.09 μM	0.5–1000 μM	[1]
Amperometric	Copper nanoparticles/CPE[a]	1.8 μM	100–1283 μM	[8]
DPV	GNPs[b], TB[c]/CPE	0.025 μM	10–0.075 μM	[9]
SPE@HPLC- FLD	-	70 ng/mL	0.07–5.75 μg/mL	[6]
SPE@LC-UV	-	2.5 ng/mL	15–25 ng/mL	[31]
SPE@HPLC-UV	-	18 ng/mL	25–1000 ng/mL	[6]
RAM@LC-UV[a]	-	1 ng/mL	5–500 ng/mL	[32]
IP-HPLC-FLD[b]	-	-	20–1500 ng/mL	[33]
FFTCV[c]	-	0.95 pg/mL	3–14900 pg/mL	[34]
MISPE@HPLC-UV[d]		10 ng/mL	0.05–100 μg/mL	[35]
MWCNT-MMIPs@UADSPME@HPLC-UV		0.31 ng/mL	0.001–2 μg/mL	[36]
DPV	MIP/AuNPs/GQD-SH/SPCE	0.035 μM	0.1–250 μM	This work

[a] Restricted Access Material Liquid Chromatography.
[b] Ion-Pair High-Performance Liquid Chromatography with Fluorescence Detection.
[c] Fast Fourier Transform with Continuous Cyclic Voltammetry.
[d] Molecularly Imprinted Solid Phase Extraction.

different SOT standards in the buffer solution (0.04 M, pH 10.0) is shown in Fig. 10. It could be seen from Fig. 10A that with increase the SOT concentration, enhanced peak current responses. For the concentration range of 0.1–250 μM, the linear regression equations were Ip $_1$(μA) = 0.0901 C_{SOT} (μM) +3.6133 and Ip_2(μA) = 0.1225 C_{SOT} (μM)+8.004 with correlation coefficient 0.9905 and 0.9902 (inset in Fig. 10B). The detection limit (3s) for SOT in the lower range region was found to be 0.035 μM (based on S/N = 3). Table 1 collected some pervious methods established for the determinations detection limit and the linear dynamic

Table 2
The selectivity of the modified electrode.

Species	Tolerance limit	Ip_1(μA)	Ip_2(μA)
Sotalol	100 μM	11.64	20.25
captopril	100 nM	11.6	20.41
glucose	70 nM	11.3	20.13
cystamine	70 nM	11.8	20.29
urea	100 nM	11.9	20.62
alanine	70 nM	12.3	20.79
ripaglinide	100 nM	11.9	20.68
terazosin	100 nM	11.8	20.57
valproate	100 nM	11.2	20.39
cysteine	50 nM	12.2	20.86

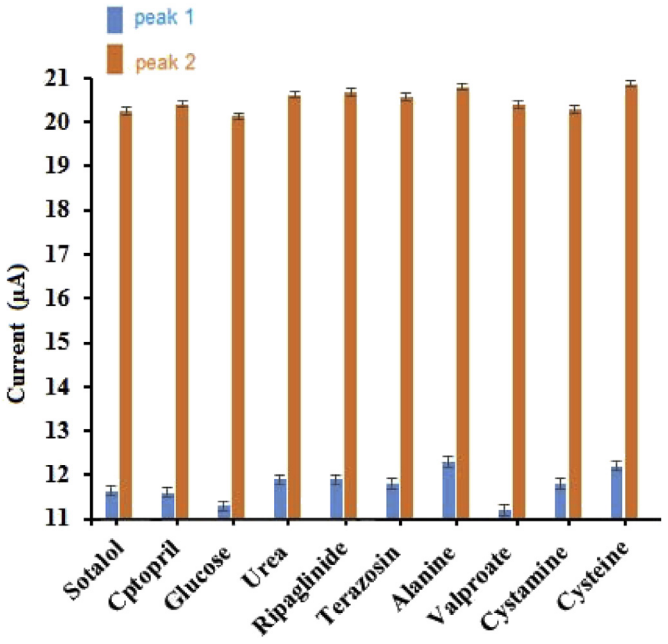

Fig. 11. The selectivity of the modified electrode in the presence similar compound such as captopril, glucose, cystamine, urea, alanine, ripaglinide, terazosin, valproate and cysteine on the surface of the MIP/AuNPs/GOD-SH/SPC electrode, in B-R buffer solution (pH 10) containing 100 μM SOT.

Table 3
Detection of SOT in real samples (n = 3).

Sample	Added (μM)	Found by electrode (μM)	Found by HPLC (μM)	RSD% electrode	RSD% HPLC	Recovery%
Blood serum	10	9.86	9.83	3.64	2.73	98.6
	20	20.34	19.46	2.96	3.84	101.7
	30	30.73	29.07	2.43	3.17	103.06
Tablet	10	9.73	10.16	2.13	4.06	97.3
	20	19.61	19.32	3.23	3.92	98.05
	30	30.11	29.40	2.69	3.57	100.3

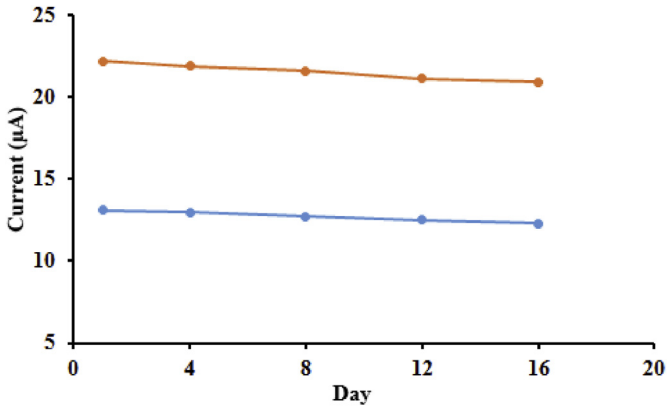

Fig. 12. The reproducibility of the modified electrode within 16 days, in B-R buffer solution (pH 10) containing 100 μM SOT.

range of SOT [1,8,9].

3.10. Interference studies

In order to assess that the presented sensor was selective to detect SOT, under the optimum conditions the sensor response was examined by various potentially interference species. Interferences from similar compound such as captopril, glucose, cystamine, urea, alanine, ripaglinide, terazosin, valproate and cysteine on the surface of the sensor at the amount of 100 μM for apiece interference in the attendance of 5 μM of SOT were used as indicators for the selectivity of the sensor in comparison with the estimate of SOT alone (Table 2 and Fig. 11). The results suggested that the proposed MIP-sensor strategy had high specificity for SOT detection.

3.11. Reproducibility of the sensor

The reproducibility of the sensor was an important factor affecting the analytical performance. To appraise the reproducibility of the presented sensor, one electrode was prepared independently with the proposed system and the electrode was stored in the laboratory and performed every day two repetitive measurements in the presence of 100 μM SOT for 14 days. The prepared sensore preserved 97% (for P_1), 97.4 % (for P_2) of its initials response after 7 days and 93.9% (for P_1), 94.4% (for P_2) after 2 week, which represented the good life time and reproducibility of the sensor for SOT analysis (Fig. 12).

3.12. Analysis of food samples

3.12.1. Analysis of real sample

To evaluation the applicability of the invented sensor for real sample analysis, the concentration of SOT in real samples was studied through means of DPV measurement and via the standard addition method. Two kinds of common real samples included tablet and human serum containing different concentrations of SOT (10, 20, 30 μM) were investigated. The recovery was specified in the range of 97.3%–103.06 % and RSD was in the range from 1.23% to 4.3%, the results as summarized are shown in Table 3. Also, Table 3 shows the results of the comparison of the differential pulse voltammetry method as a proposed method and the high performance liquid chromatographymethod for statistical estimation.

4. Conclusion

Briefly, electrochemical sensors offer a crucial analytical instrument as demand for selective, sensitive, and fast determination of analytes. This work showed the application of a SPCE modified with AuNPs, SH-GQD and MIP for the determination of SOT. Utilizing of the N-GQDs as a sub layer in preparation of the nanocomposite can create more surface area for immobilization of further substrate on the modified electrode surface. Also, the AuNPs have been immobilized onto the SH groups of GQDs through bonding formation of Au–S. This bonding formation in resulted the acceleration of the electron transfer kinetics, improved the electrochemical signal, and also increased the adsorption of the SOT in surface the sensor. Drawbacks associated to MIP processes, such as long times for bulk polymerization and long elution steps for analyte removal from the polymeric tissue, are avoided by using a fabricated electrochemical sensor with stability, sensitivity, selectivity, simplicity, good repeatability and Inexpensive. Also, this electrochemical sensor had a low detection limit, wide linear range, and it was ascertain to be an efficient, tool to detect SOT in real samples with satisfactory recoveries.

Declarations

Author contribution statement

Mahmoud Roushani: Conceived and designed the experiments; Analyzed and interpreted the data; Contributed reagents, materials, analysis tools or data; Wrote the paper.

Zeynab Jalilian: Performed the experiments; Analyzed and interpreted the data; Wrote the paper.

Azizollah Nezhadali: Contributed reagents, materials, analysis tools or data.

Funding statement

This research did not receive any specific grant from funding agencies in the public, commercial, or not-for-profit sectors.

Competing interest statement

The authors declare no conflict of interest.

Additional information

No additional information is available for this paper.

References

[1] A.A. Ensafi, A.R. Allafchian, B. Rezaei, R. Mohammadzadeh, Characterization of carbon nanotubes decorated with $NiFe_2O_4$ magnetic nanoparticles as a novel electrochemical sensor: application for highly selective determination of sotalol using voltammetry, Mater. Sci. Eng. C 33 (2013) 202–208.

[2] H. Zhang, J. Yang, L. Du, C.H. Li, H. Wu, Determination of sotalol by fluorescence quenching method, Anal. Methods 3 (2011) 1156.

[3] J. Boutagy, G.M. Shenfield, Simplified procedure for the determination of sotalol in plasma by high-performance liquid chromatography, J. Chromatogr. 565 (1991) 523–528.

[4] P.J. Neuvonen, E. Elonen, T. Vuorenmaa, M. Laakso, Prolonged Q-T interval and severe tachyarrhythmias, common features of sotalol intoxication, Eur. J. Clin. Pharmacol. 20 (1981) 85–89.

[5] M.J. Bartek, M. Vekshteyn, M.P. Boarman, D.G. Gallo, Liquid chromatographic determination of sotalol in plasma and urine employing solid-phase extraction and fluorescence detection, J. Chromatogr. 421 (1987) 309–318.

[6] M. Schlauch, K. Fulde, A.W. Frahm, Enantioselective determination of (R)- and (S)-sotalol in human plasma by on-line coupling of a restricted-access material precolumn to a cellobiohydrolase I-based chiral stationary phase, J. Chromatogr. B 775 (2002) 197–207.

[7] E. Badaloni, I. Dacquarica, F. Gasparrini, S. Lalli, D. Misiti, F. Pazzucconi, C.R. Sirtori, Enantioselective liquid chromatographic-electrospray mass spectrometric assay of β-adrenergic blockers: application to a pharmacokinetic study of sotalol in human plasma, J. Chromatogr. B 796 (2003) 45–54.

[8] H. Heli, A. Jabbari, M. Zarghan, A.A. Moosavi-Movahedi, Copper nanoparticles–carbon microparticles nanocomposite for electrooxidation and sensitive detection of sotalol, Sens. Actuators, B 140 (2009) 245–251.

[9] M.A. Mohamed, A.M. Fekry, M.A. El-Shal, C.E. Banks, Incorporation of tetrazolium blue (TB)/gold nanoparticles (GNPs) into carbon paste electrode: application as an electrochemical sensor for the sensitive and selective determination of sotalol in micellar medium, Electroanalysis 29 (2017) 1–9.

[10] A. Nezhadali, M. Mojarrab, Computational study and multivariate optimization of hydrochlorothiazide analysis using molecularly imprinted polymer electrochemical sensor based on carbon nanotube/polypyrrole film, Sensor. Actuator. B Chem. 190 (2014) 829–837.

[11] N. Atar, M. Lütfi Yola, T. Eren, Sensitive determination of citrinin based on molecular imprinted electrochemical sensor, Appl. Surf. Sci. 362 (2016) 315–322.

[12] A.M. Ruela, E.C. Figueiredo, G.R. Pereira, Molecularly imprinted polymers as nicotine transdermal delivery systems, Chem. Eng. J. 248 (2014) 1–8.

[13] M. Roushani, A. Nezhadali, Z. Jalilian, A. Azadbakht, Development of novel electrochemical sensor on the base of molecular imprinted polymer decorated on SiC nanoparticles modified glassy carbon electrode for selective determination of loratadine, Mater. Sci. Eng. C 71 (2017) 1106–1114.

[14] M. Roushani, Z. Jalilian, Development of electrochemical sensor based on glassy carbon electrode modified with a molecularly imprinted copolymer and its application for detection of repaglinide, Electroanalysis 30 (2018) 1–8.

[15] M. Roushani, A. Nezhadali, Z. Jalilian, An electrochemical chlorpyrifos aptasensor based on the use of a glassy carbon electrode modified with an electropolymerized aptamer-imprinted polymer and gold nanorods, Microchimica Acta 185 (2018) 551–558.

[16] Z. Taleat, A.R. Khoshroo, M. Mazloum-Ardakani, Screen-printed electrodes for biosensing, a review Microchim Acta 181 (2014) 865–891.

[17] M. Roushani, Z. Jalilian, A. Nezhadali, A novel electrochemical sensor based on electrode modified with gold nanoparticles and molecularly imprinted polymer for rapid determination of terazosin, Colloids Surf., B 172 (2018) 594–600.

[18] M. Lütfi Yola, C. Göde, N. Atar, Molecular imprinting polymer with Polyoxometalate/carbon nitride nanotubes for electrochemical recognition of bilirubin, Electrochim. Acta 246 (2017) 135–140.

[19] H. Wan, Q. Sun, H. Li, F. Sun, N. Hu, P. Wang, Screen-printed gold electrode with gold nanoparticles modification for simultaneous electrochemical determination of lead and copper, Sens. Actuators, B 209 (2015) 336–342.

[20] S.X. Lee, H.N. Lim, I. Ibrahim, A. Jamil, A. Pandikumar, N.M. Huang, Horseradish peroxidase-labeled silver/reduced graphene oxide thin film-modified screen-printed electrode for detection of carcinoembryonic antigen, Biosens. Bioelectron. 89 (2017) 673–680.

[21] G. Sun, J. Lu, S. Ge, X. Song, J. Yu, M. Yan, J. Huang, Ultrasensitive electrochemical immunoassay for carcinoembryonic antigen based on three-dimensional macroporous gold nanoparticles/graphene composite platform and multienzyme functionalized nanoporous silver label, Anal. Chim. Acta 775 (2013) 85–92.

[22] L.A. Ponomarenko, F. Schedin, M.I. Katsnelson, R. Yang, E.W. Hill, K.S. Novoselov, A.K. Geim, Chaotic Dirac billiard in graphene quantum dots, Science 320 (2008) 356–358.

[23] K. Ghanbari, M. Roushani, A. Azadbakht, Ultra-sensitive aptasensor based on a GQD nanocomposite for detection of hepatitis C virus core antigen, Anal. Biochem. 534 (2017) 64–69.

[24] Z. Lur, X. Chen, Y. Wang, X. Zheng, C.M. Li, Aptamer based fluorescence recovery assay for aflatoxin B1 using a quencher system composed of quantum dots and graphene oxide, Microchimica Acta 182 (2015) 571–578.

[25] M. Roushani, M. Mavaei, H.R. Rajabi, Graphene quantum dots as novel and green nano-materials for the visible-light-driven photocatalytic degradation, J. Mol. Catal. B Enzym. 409 (2015) 102–109.

[26] I.L. Medintz, H.T. Uyeda, E.R. Goldman, H. Mattoussi, Quantum dot bioconjugates for imaging. Labelling and sensing, Nat. Mater. 4 (2005) 435–446.

[27] M. Roushani, Z. Abdi, Novel electrochemical sensor based on graphene quantum dots/riboflavin nanocomposite for the detection of persulfate, Sensor. Actuator. B Chem. 201 (2014) 503–510.

[28] M. Lütfi Yolaa, N. Atar, A novel detection approach for serotonin by graphene quantum dots/two-dimensional (2D) hexagonal boron nitride nanosheets with molecularly imprinted polymer, Appl. Surf. Sci. 458 (2018) 648–655.

[29] L. Minati, S. Torrengo, D. Maniglio, C. Migliaresi, G. Speranza, Luminescent graphene quantum dots from oxidized multi-walled carbon nanotubes, Mater. Chem. Phys. 137 (2012) 12–16.

[30] A. Valipour, M. Roushani, Using silver nanoparticle and thiol grapheme quantum dots nanocomposite as a substratum to load antibody for detection of hepatitis C virus core antigen: electrochemical oxidation of riboflavin was used as redox probe, Biosens. Bioelectron. 89 (2016) 946–951.

[31] P. Chiap, A. Ceccato, B. Miralles Buraglia, B. Boulanger, P. Hubert, J. Crommen, Development and validation of an automated method for the liquid chromatographic determination of sotalol in plasma using dialysis and trace enrichment on a cation-exchange pre-column as on-line sample preparation, J. Pharm. Biomed. Anal. 24 (2001) 801–814.

[32] O. Rbeida, B. Christiaens, P. Chiap, P. Hubert, D. Lubda, K.S. Boos, J. Crommen, Fully automated LC method for the determination of sotalol in human plasma using restricted access material with cation exchange properties for sample clean-up, J. Pharm. Biomed. Anal. 32 (2003) 829–838.

[33] A. Zarghi, S.M. Foroutan, A. Shafaati, A. Khoddam, Development an ion-pair liquid chromatographic method for determination of sotalol in plasma using a monolithic column, J. Pharm. Biomed. Anal. 41 (2006) 1433–1437.

[34] P. Norouzi, M.R. Ganjali, A.S. Emami Meibodi, B. Larijani, Sotalol nanolevel detection at an Au microelectrode in flowing solutions, Russ. J. Electrochem. 44 (2008) 1024–1030.

[35] S. Ansari, M. Karimi M, Synthesis and application of molecularly imprinted polymer for highly selective solid phase extraction trace amount of sotalol from human urine samples: optimization by central composite design (CCD), Med. Chem. Res. 26 (2017) 2477–2490.

[36] S. Ansari, S. Masoum, Multi-walled carbon nanotube-based magnetic molecularly imprinted polymer as a highly selective sorbent for ultrasonic-assisted dispersive solid-phase microextraction of sotalol in biological fluids, Analyst 2018 (143) (2018) 2862–2875.